PHYSICAL REVIEW B **96**, 161114(R) (2017)

Identification of Si-vacancy related room-temperature qubits in 4*H* silicon carbide

Viktor Ivády,[1,2,*] Joel Davidsson,[1] Nguyen Tien Son,[1] Takeshi Ohshima,[3] Igor A. Abrikosov,[1,4] and Adam Gali[2,5,†]

[1]*Department of Physics, Chemistry and Biology, Linköping University, SE-581 83 Linköping, Sweden*

[2]*Wigner Research Centre for Physics, Hungarian Academy of Sciences, P.O. Box 49, H-1525 Budapest, Hungary*

[3]*National Institutes for Quantum and Radiological Science and Technology, 1233 Watanuki, Takasaki, Gunma 370-1292, Japan*

[4]*Materials Modeling and Development Laboratory, National University of Science and Technology "MISIS," 119049 Moscow, Russia*

[5]*Department of Atomic Physics, Budapest University of Technology and Economics, Budafoki út 8., H-1111 Budapest, Hungary*

(Received 22 August 2017; published 27 October 2017)

The identification of a microscopic configuration of point defects acting as quantum bits is a key step in the advance of quantum information processing and sensing. Among the numerous candidates, silicon-vacancy related centers in silicon carbide (SiC) have shown remarkable properties owing to their particular spin-3/2 ground and excited states. Although, these centers were observed decades ago, two competing models, the isolated negatively charged silicon vacancy and the complex of negatively charged silicon vacancy and neutral carbon vacancy [Phys. Rev. Lett. **115**, 247602 (2015)], are still argued as an origin. By means of high-precision first-principles calculations and high-resolution electron spin resonance measurements, we here unambiguously identify the Si-vacancy related qubits in hexagonal SiC as isolated negatively charged silicon vacancies. Moreover, we identify the Si-vacancy qubit configurations that provide room-temperature optical readout.

DOI: 10.1103/PhysRevB.96.161114

Point defects in solids acting as quantum bits (qubits) are a highly promising platform for quantum information processing (QIP) and nanoscale sensor applications where typically their electron spin provides the functional quantum states. There are qubits that have long electron spin coherence times [1–5], and some of them have been demonstrated to persist up to room temperature [1,4]. These electron spins can be optically initialized and read out [2,6–9], making them very attractive candidates for QIP and related applications [10–12]. Among these qubits, silicon-vacancy related defects in hexagonal polytypes of SiC, such as 4*H*- and 6*H*-SiC, have shown favorable spin properties [13,14], demonstrated even at a single defect level at room temperature [4]. Two and three different silicon-vacancy related centers were observed in 4*H*- and 6*H*-SiC, where the corresponding photoluminescence (PL) lines are denoted as V1 and V2, and V1, V2, and V3, [15,16], respectively. The V2 line in 4*H*-SiC [4] and the V2 and V3 lines in 6*H*-SiC [13] are sufficiently strong to observe their corresponding electron spin via optically detected magnetic resonance (ODMR) measurements at room temperature. In particular, it has been demonstrated that the V2 color center in 4*H*-SiC can be used for magnetometer [17–20] and nanoscale thermometer [21] applications and as a room-temperature maser [14].

Today, it is widely accepted that V1-V3 PL lines and T_{V1}-T_{V3} electron paramagnetic resonance (EPR) signals in 4*H*- and 6*H*-SiC are related to spin-3/2 negatively charged silicon vacancies [22–25]. On the other hand, the actual microscopic configuration of these vacancy related centers is still debated. The unanswered question is whether these centers are isolated silicon vacancies [$V_{Si}(-)$ as model I] [23,25,26] or axial symmetric defect pairs, including a negatively charged silicon vacancy and a proximate neutral carbon vacancy [14,27] [$V_{Si}(-) + V_C(0)$ as model II]; see Fig. 1. An important difference between the two models is how the observed finite zero-field splitting (ZFS) of the ground-state spin sublevels is explained. In model I, it is assumed that the C_{3v} symmetric crystal field, allowing nonzero ZFS [26], is strong enough to cause a finite ZFS that accounts for the observations. A recent theoretical estimate on the ZFS of the V2 center in 4*H*-SiC supports this assumption [28]. We note that Mizuochi and co-workers [29] associated the V2 center particularly with $V_{Si}(-)$ at the *h* site by comparing the similarities of V1-V2 and V1-V3 signals in 4*H*- and 6*H*-SiC, respectively. Model II, on the other hand, uses the nondistorted silicon-vacancy model [14,22], where close to T_d symmetry with negligible ZFS is assumed for an isolated $V_{Si}(-)$ in hexagonal SiC. In this model, a proximate neutral carbon vacancy in a symmetrical configuration is assumed [see, for example, the model of the V2 center in 4*H*-SiC [14] in Fig. 1(c)] that lowers the symmetry of the silicon vacancy, thus causing a finite ZFS. In a recent experiment on rhombic 15*R*-SiC [27], silicon-vacancy related centers were reported with similar characteristics to those in hexagonal SiC. Using electron nuclear double-resonance (ENDOR) measurements, negative ^{29}Si hyperfine coupling constants, i.e., negative electron spin density, were observed for the V2 center in 15*R*-SiC. As a proof of model II, this observation was attributed to the hyperfine coupling of the weakly negatively polarized silicon nuclei around the carbon vacancy [27]. The identification of the microscopic structure of the V1-V2 centers in 4*H* SiC, i.e., validating one of these models, is essential for an appropriate theoretical description and for controlled single defect fabrication purposes.

In this Rapid Communication, we show by means of high-precision first-principles calculations that the silicon-vacancy–carbon-vacancy pair model of the V2 center in 4*H*-SiC is a metastable configuration that has a spin-1/2 ground state without any zero-field splitting and a hyperfine signature that differs significantly from the experiment. Furthermore, we demonstrate by theoretical simulations and high-resolution EPR measurements that the isolated silicon-vacancy model accounts for the majority of the observed magneto-optical

*vikiv@ifm.liu.se

†gali.adam@wigner.mta.hu

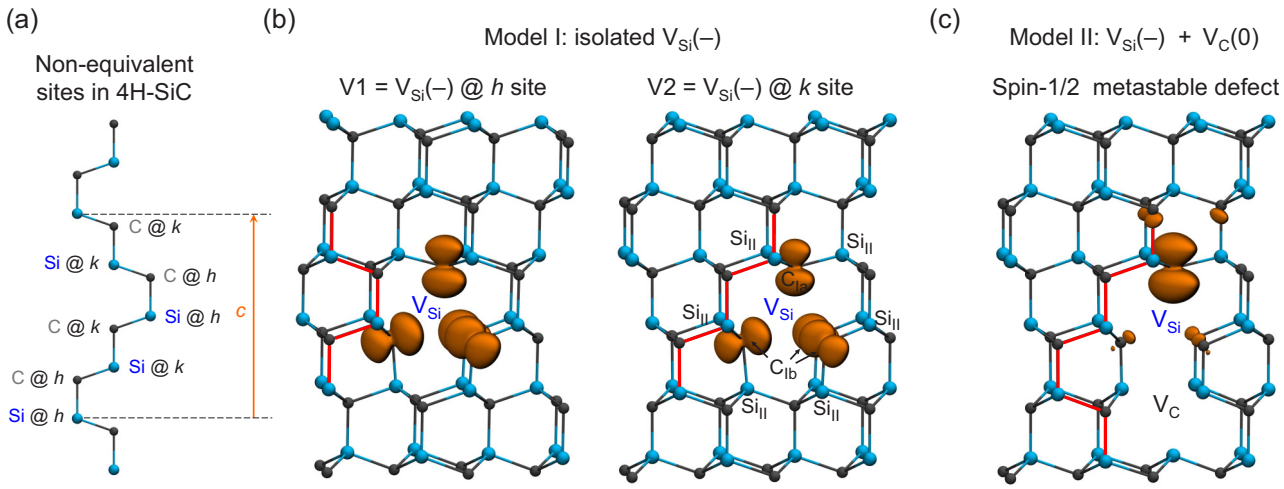

FIG. 1. Models of V1-V2 silicon-vacancy related qubits in 4*H*-SiC. (a) Nonequivalent atomic sites, i.e., a quasihexagonal *h* site and a quasicubic *k* site, in the primitive cell of 4*H*-SiC. (b) Isolated vacancy model and the assignment of V1-V2 centers to the different silicon-vacancy configurations in 4*H*-SiC. (c) Vacancy pair model of V2 center [14]. In (b) and (c), red lines highlight the stacking of the Si-C double layers to help identify different configurations of silicon and carbon vacancies. Orange lobes show the spin density of the defects. Based on our first-principles results, the isolated vacancy model in (b) can be assigned to the V1 and V2 centers in 4*H*-SiC.

properties of the V1-V2 centers in 4*H*-SiC. Especially, the simulated zero-phonon-line (ZPL) energies, the nonzero ZFS values, and the hyperfine structure that includes ^{29}Si hyperfine values that correspond to negative electron spin polarization are all in good agreement with the observations. Based on these results, we identify the V1-V2 centers in 4*H*-SiC as isolated negatively charged silicon vacancies. Furthermore, we identify the room-temperature V2 Si-vacancy qubit at the *k* site in 4*H*-SiC, in contrast to previous assignments.

In our first-principles point defect characterization study, we apply the density functional theory (DFT) and supercell method to model single point defects. We apply a plane-wave basis set of 420 eV and standard projector augmented-wave [30] potentials as implemented in the VASP code [31,32]. For ZPL and hyperfine tensor calculations we use the Heyd-Scuseria-Ernzerhof (HSE06) [33,34] hybrid exchange-correlation functional that has already demonstrated its predictive power for optical [35,36] and hyperfine properties [37]. In the zero-field-splitting calculations we use the Perdew-Burke-Ernzerhof (PBE) [38] functional that provides accurate results for defects in wide band gap semiconductors [39]. According to previous theoretical ZFS studies on the NV center in diamond [39,40], divacancy in SiC [40], and our present results, the theoretical ZFS values have ∼16 MHz mean absolute error when compared with the experiment. Nevertheless, the ZFS values sensitively depend on the fine details of the crystal field, thus the tendencies observed in the calculated values can still be used for the identification of symmetrically nonequivalent configurations of the point defects (see, for example, Ref. [40]). For the sake of high numerical accuracy [41], we employ a 1532-atom 4*H*-SiC supercell with Γ-point sampling of the Brillouin zone. For structural optimization with the HSE06 functional in these large supercells, the plane-wave cutoff energy is slightly reduced to 390 eV, and a force criterion of 0.01 eV/Å is applied. As the supercell size, ≈30 Å in the *c* direction, is sufficiently large to properly accommodate both the isolated vacancy (model I) and the defect pair (model II), the results of these calculations are comparable.

High-precision EPR measurements in a 4*H*-SiC sample were performed on a Bruker X-band EPR spectrometer. A high-purity semi-insulating (HPSI) bulk sample with a large size was irradiated by 2 MeV electrons to a fluence of 8×10^{18} cm^{-2} at room temperature and annealed at ∼400 °C in order to remove the interference of other EPR centers related to interstitial defects. EPR measurements were performed in the dark at room temperature. For further details on EPR experiments in 4*H* and 6*H*-SiC, see Ref. [42].

First, we carry out a high-precision first-principles calculation on model II. We consider the nearest $V_{Si}(-) + V_C(0)$ pair not sharing the same Si-C bilayer [see Fig. 1(c)], which is the suggested configuration for the V2 center in 4*H*-, 6*H*-, and 15*R*-SiC [14,27]. In the simulations, we observe a notable interaction between the vacancies that results in a weakly bonded defect pair with an electronic structure that significantly differs from the electronic structure of the isolated silicon vacancy (see Fig. 2). In the tight-binding

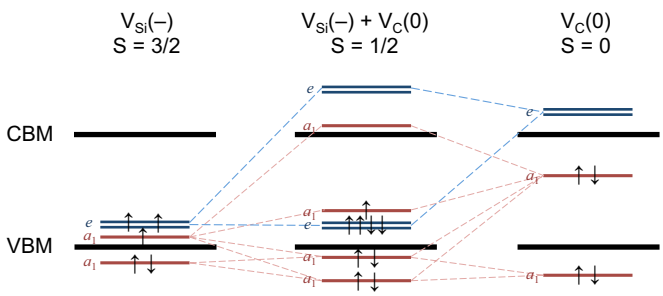

FIG. 2. Electronic structure of $V_{Si}(-) + V_C(0)$ complex: Defect molecule diagram analysis with the states of the isolated silicon and carbon vacancies. The positions of one-particle states for $V_{Si}(-)$ and $V_{Si}(-) + V_C(0)$ reflect the results of our *ab initio* calculations. For the electronic structure of the carbon vacancy in 4*H*-SiC, see Ref. [43].

picture, both isolated $V_{Si}(-)$ and isolated $V_C(0)$ possess two nondegenerate a_1 states and a doubly degenerate e state. In the case of isolated $V_{Si}(-)$, an a_1 state and an e state appear in the band gap with increasing energy. In the $V_{Si}(-) + V_C(0)$ pair, the e states of the vacancies form a weakly bounding e state that falls into the band gap and is mainly localized on the silicon-vacancy site. Beside this state, an a_1 state of antibonding nature appears into the band gap slightly above the e state. Altogether, five electrons can be found in the band gap that fully occupy the lower lying e state and partially occupy the a_1 state. The ground state of the $V_{Si}(-) + V_C(0)$ pair defect is thus spin-1/2 [see the spin density in Fig. 1(c)]. The hyperfine signature of the defect substantially deviates from the V1-V2 centers' hyperfine signature in 4H-SiC [42]. Furthermore, by comparing the formation energy of model II and the negatively charged divacancy (immediate neighbor vacancies sharing the same Si-C bilayer), we find that the latter is lower in energy by 1.58 eV, showing that model II is a metastable configuration of the negatively charged divacancy, which presumably anneals out at the temperatures where carbon vacancies are mobile [44]. Based on these results we argue that the silicon-vacancy–carbon-vacancy pair model is not appropriate for the silicon-vacancy related centers in SiC.

We further note that the negative anisotropic ^{29}Si hyperfine splitting in the range of 1.3–2.2 MHz observed by ENDOR [27] can be explained by isolated $V_{Si}(-)$ and it is not evidence of the presence of a carbon vacancy. As the spin density is the fingerprint of a complex many-body wave function, sign changes in the spin density may occur even for a simple point defect, for instance, the NV center diamond [35]. As our DFT simulations can capture these effects, we investigate the hyperfine interactions of both ^{29}Si and ^{13}C nuclei up to 7.8 Å distance from the isolated silicon vacancy (model I) [42]. We find negative anisotropic ^{29}Si hyperfine splitting in the order of a few MHz for both silicon-vacancy configurations in 4H-SiC. In particular, $A_z = -1.3$ to -2.1 MHz is found for several Si sites 6.1 Å away from the silicon vacancy and $A_z = -5.1$ MHz is found for one Si site 5.0 Å away from V_{Si} at the k site [42].

Figure 3 shows a high-resolution EPR spectrum in 4H-SiC measured at 292 K in the dark for $B \parallel c$. With low MW and low-field modulation, the overlapping between the ZFS components of the T_{V1a} center (with a splitting of ∼3.66 G) and the hyperfine structure due to the interaction with the nuclear spin of one ^{29}Si among 12 equivalent Si in the second neighbor (∼3 G) can be resolved. The observed ZFS and the hyperfine constants of the interaction with one C and three C in the nearest neighbor and with 12 Si in the second neighbor for the T_{V1a} and T_{V2a} centers in 4H-SiC are given in Table I. Corresponding data for 6H-SiC can be found in Ref. [42]. Furthermore, a small hyperfine splitting of ≈0.8 G (≈2.2 MHz) due to the hyperfine interaction with ^{29}Si nuclei in further neighbor shells beyond the second neighbor is also observed in 4H-SiC (see the inset in Fig. 3). Note that our first-principles calculation on the isolated silicon vacancy in 4H-SiC can account for this splitting (see the negative hyperfine coupling constants above and Ref. [42]). Furthermore, the magnitude of the negative hyperfine coupling constants reported for the silicon-vacancy related centers in 15R-SiC [27] is similar to the ≈0.8 G (≈2.2 MHz) splitting observed in our EPR

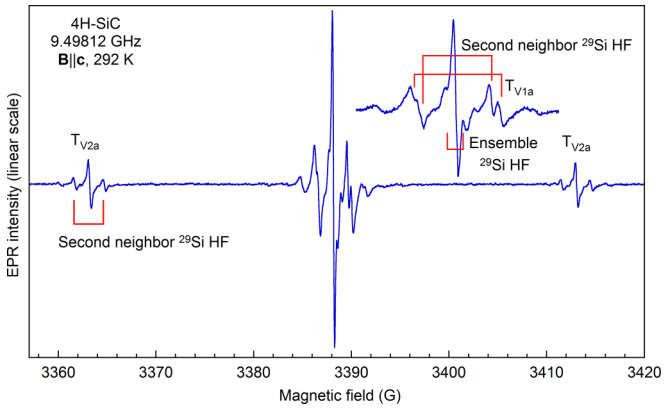

FIG. 3. EPR spectra of the T_{V1a} and T_{V2a} centers in 4H-SiC measured in the dark at 292 K for $B \parallel c$ using a low microwave power (MW) of 2 μW and a low modulation field of 0.01 G. In an extended magnetic field scale, the inset shows the ZFS of T_{V1a}, which partly overlaps with the Si hyperfine structure, and a small Si hyperfine splitting of ∼0.8 G (∼2.2 MHz).

results in 4H-SiC. Since the electronic structure of the isolated vacancy in 15R-SiC is akin to their counterparts' electronic structure in 4H-SiC, a similar negative spin density shell, resulting in negative ^{29}Si hyperfine constants, should form around the silicon vacancies in 15R-SiC. Our results indicate that the isolated $V_{Si}(-)$ can account for the ENDOR signatures recorded in 15R-SiC fairly well.

Next, we thoroughly investigate the isolated $V_{Si}(-)$ model in 4H-SiC. The multiplet structure of these defects includes a $^4A_2$ ground state, low-energy $^4A_2$ and ^4E optically allowed excited states, and other spin-1/2 shelving states between the ground and optical excited states [28]. Accordingly, in our first-principles calculations, we consider the $^4A_2$ ground state and the lowest-energy optically excited state, either the $^4A_2$ or the ^4E state. We calculate the ground-state ZFS values, ZPL

TABLE I. Theoretical and experimental magneto-optical data for V1 and V2 centers in 4H-SiC. The hyperfine splitting at $B \parallel c$ was determined for the first neighbor ^{13}C nuclei on ($1 \times C_{Ia}$) and out ($3 \times C_{Ib}$) of the symmetry axis of the isolated silicon vacancy and the averaged hyperfine splitting for the 12 second neighbor ^{29}Si sites ($12 \times \tilde{Si}_{II}$). See the considered nuclei sites in Fig. 1(b). Experimental ZPL energies were reported in Ref. [16] while the ZFS and the resolvable hyperfine values are determined by our EPR measurements (see Fig. 3). There is good agreement between theory and experiment supporting the isolated silicon-vacancy model of V1-V2 centers.

Center/			Hyperfine splitting (MHz)		
Configuration	ZFS (MHz)	ZPL (eV)	$1 \times C_{Ia}$	$3 \times C_{Ib}$	$12 \times \tilde{Si}_{II}$
		Experiment			
V1	2.6	1.438	79.9	39.2	8.2
V2	35.0	1.352	80.4	37.0	8.4
		Theory			
V_{Si}^- at h	18.3	1.541	85.5	40.6	7.7
V_{Si}^- at k	33.3	1.443	84.7	38.7	7.9

line energies, and ground-state hyperfine splitting for $B \parallel c$ and compare them with existing ZPL data and with the results of our EPR ZFS and hyperfine splitting measurements. Our theoretical and experimental ZFS values are given in Table I. Importantly, the theoretically predicted ZFS is nonzero for all the symmetrically nonequivalent vacancy configurations. In agreement with previous theoretical estimates [28], these results disprove the existence of an undistorted T_d symmetric silicon vacancy [22] in 4H-SiC, which was one of the basic assumptions of model II [14]. Furthermore, both the calculated ZPL energies and the hyperfine values are in good agreement with the experimental data.

Finally, since not all of the silicon-vacancy centers have a room-temperature ODMR signal, they have a different potential for qubit applications. The V2 center in 4H-SiC exhibits an observable ODMR signal even at room temperature and its spin ensemble has been used for magnetometry [17–20]. Thus, improving the brightness and ODMR contrast of these single emitters is promising for room-temperature nanoscale magnetometry of biological molecules and quantum information processing applications [4,10]. For a proper theoretical description and single defect engineering, the actual configuration of this center should be determined. Therefore, here we assign the symmetrically nonequivalent isolated silicon-vacancy configurations [see Fig. 1(a)] to the V1-V2 centers in 4H-SiC. Note that such an assignment requires an especially high precision from both the theoretical and the experimental results. As can be seen in Table I, the ZFS results, the ZPL energies, and the vast majority of hyperfine constants in the first and second shell around the vacancy [45] support the identification of the V1 center as $V_{Si}(-)$ at the h site and the V2 center as $V_{Si}(-)$ at the k site. Accordingly, we assign the V1 and V2 centers in 4H-SiC to the h and k configuration of $V_{Si}(-)$, respectively. Note that this assignment is in contrast to the previously suggested identification [16,29] that relies on a comparison of 4H and 6H-SiC magneto-optical spectra. This approach, however, can be misleading for defect configuration identification in hexagonal SiC [46].

In summary, we investigated the microscopic origin of the V1-V2 centers in 4H-SiC. We demonstrated by first-principles calculations that the silicon-vacancy–carbon-vacancy defect is metastable and possesses an $S = 1/2$ ground state, in stark contrast to the properties of the V1-V2 centers. We showed, however, that the isolated negatively charged silicon vacancy can accurately reproduce the reported magneto-optical data of these centers, including the hyperfine signatures of ^{29}Si nuclear spins. Furthermore, we identified the room-temperature V2 qubit as $V_{Si}(-)$ at the k site in 4H-SiC.

Support from the Knut & Alice Wallenberg Foundation project Strong Field Physics and New States of Matter 2014-2019 (COTXS), the Grant of the Ministry of Education and Science of the Russian Federation (Grant No. 14.Y26.31.0005), the Swedish Research Council (VR 2016-04068), the Carl-Trygger Stiftelse för Vetenskaplig Forskning (CTS 15:339), JSPS KAKENHI A 17H01056, and the Hungarian NKFIH Grant No. NVKP_16-1-2016-0152958 is acknowledged. The calculations were performed on resources provided by the Swedish National Infrastructure for Computing (SNIC 2016/1-528) at the National Supercomputer Centre (NSC) and by Linköping University (LiU-2015-00017-60).

[1] G. Balasubramanian, P. Neumann, D. Twitchen, M. Markham, R. Kolesov, N. Mizuochi, J. Isoya, J. Achard, J. Beck, J. Tissler, V. Jacques, P. R. Hemmer, F. Jelezko, and J. Wrachtrup, Nat. Mater. **8**, 383 (2009).

[2] W. F. Koehl, B. B. Buckley, F. J. Heremans, G. Calusine, and D. D. Awschalom, Nature (London) **479**, 84 (2011).

[3] D. J. Christle, A. L. Falk, P. Andrich, P. V. Klimov, J. U. Hassan, N. T. Son, E. Janzén, T. Ohshima, and D. D. Awschalom, Nat. Mater. **14**, 160 (2015).

[4] M. Widmann, S.-Y. Lee, T. Rendler, N. T. Son, H. Fedder, S. Paik, L.-P. Yang, N. Zhao, S. Yang, I. Booker, A. Denisenko, M. Jamali, S. A. Momenzadeh, I. Gerhardt, T. Ohshima, A. Gali, E. Janzén, and J. Wrachtrup, Nat. Mater. **14**, 164 (2015).

[5] B. C. Rose, D. Huang, Z.-H. Zhang, A. M. Tyryshkin, S. Sangtawesin, S. Srinivasan, L. Loudin, M. L. Markham, A. M. Edmonds, D. J. Twitchen, S. A. Lyon, and N. P. de Leon, arXiv:1706.01555.

[6] F. Jelezko and J. Wrachtrup, Phys. Status Solidi A **203**, 3207 (2006).

[7] B. B. Buckley, G. D. Fuchs, L. C. Bassett, and D. D. Awschalom, Science **330**, 1212 (2010).

[8] L. Robledo, L. Childress, H. Bernien, B. Hensen, P. F. A. Alkemade, and R. Hanson, Nature (London) **477**, 574 (2011).

[9] A. L. Falk, B. B. Buckley, G. Calusine, W. F. Koehl, V. V. Dobrovitski, A. Politi, C. A. Zorman, P. X.-L. Feng, and D. D. Awschalom, Nat. Commun. **4**, 1819 (2013).

[10] P. Baranov, I. Il'in, E. Mokhov, M. Muzafarova, S. Orlinskii, and J. Schmidt, JETP Lett. **82**, 441 (2005).

[11] A. Gali, Phys. Status Solidi B **248**, 1337 (2011).

[12] J. R. Weber, W. F. Koehl, J. B. Varley, A. Janotti, B. B. Buckley, C. G. Van de Walle, and D. D. Awschalom, Proc. Natl. Acad. Sci. USA **107**, 8513 (2010).

[13] D. Riedel, F. Fuchs, H. Kraus, S. Väth, A. Sperlich, V. Dyakonov, A. A. Soltamova, P. G. Baranov, V. A. Ilyin, and G. V. Astakhov, Phys. Rev. Lett. **109**, 226402 (2012).

[14] H. Kraus, V. A. Soltamov, D. Riedel, S. Väth, F. Fuchs, A. Sperlich, P. G. Baranov, V. Dyakonov, and G. V. Astakhov, Nat. Phys. **10**, 157 (2014).

[15] E. Sörman, N. T. Son, W. M. Chen, O. Kordina, C. Hallin, and E. Janzén, Phys. Rev. B **61**, 2613 (2000).

[16] M. Wagner, B. Magnusson, W. M. Chen, E. Janzén, E. Sörman, C. Hallin, and J. L. Lindström, Phys. Rev. B **62**, 16555 (2000).

[17] S.-Y. Lee, M. Niethammer, and J. Wrachtrup, Phys. Rev. B **92**, 115201 (2015).

[18] D. Simin, V. A. Soltamov, A. V. Poshakinskiy, A. N. Anisimov, R. A. Babunts, D. O. Tolmachev, E. N. Mokhov, M. Trupke, S. A. Tarasenko, A. Sperlich, P. G. Baranov, V. Dyakonov, and G. V. Astakhov, Phys. Rev. X **6**, 031014 (2016).

[19] M. Niethammer, M. Widmann, S.-Y. Lee, P. Stenberg, O. Kordina, T. Ohshima, N. T. Son, E. Janzén, and J. Wrachtrup, Phys. Rev. Appl. **6**, 034001 (2016).

[20] C. J. Cochrane, J. Blacksberg, M. A. Anders, and P. M. Lenahan, Sci. Rep. **6**, 37077 (2016).
[21] A. N. Anisimov, D. Simin, V. A. Soltamov, S. P. Lebedev, P. G. Baranov, G. V. Astakhov, and V. Dyakonov, Sci. Rep. **6**, 33301 (2016).
[22] T. Wimbauer, B. K. Meyer, A. Hofstaetter, A. Scharmann, and H. Overhof, Phys. Rev. B **56**, 7384 (1997).
[23] N. Mizuochi, S. Yamasaki, H. Takizawa, N. Morishita, T. Ohshima, H. Itoh, and J. Isoya, Phys. Rev. B **66**, 235202 (2002).
[24] S. B. Orlinski, J. Schmidt, E. N. Mokhov, and P. G. Baranov, Phys. Rev. B **67**, 125207 (2003).
[25] N. Mizuochi, S. Yamasaki, H. Takizawa, N. Morishita, T. Ohshima, H. Itoh, T. Umeda, and J. Isoya, Phys. Rev. B **72**, 235208 (2005).
[26] E. Janzén, A. Gali, P. Carlsson, A. Gällström, B. Magnusson, and N. T. Son, Physica B (Amsterdam) **404**, 4354 (2009).
[27] V. A. Soltamov, B. V. Yavkin, D. O. Tolmachev, R. A. Babunts, A. G. Badalyan, V. Y. Davydov, E. N. Mokhov, I. I. Proskuryakov, S. B. Orlinskii, and P. G. Baranov, Phys. Rev. Lett. **115**, 247602 (2015).
[28] O. O. Soykal, P. Dev, and S. E. Economou, Phys. Rev. B **93**, 081207 (2016).
[29] N. Mizuochi, S. Yamasaki, H. Takizawa, N. Morishita, T. Ohshima, H. Itoh, and J. Isoya, Phys. Rev. B **68**, 165206 (2003).
[30] P. E. Blöchl, Phys. Rev. B **50**, 17953 (1994).
[31] G. Kresse and J. Hafner, Phys. Rev. B **49**, 14251 (1994).
[32] G. Kresse and J. Furthmüller, Phys. Rev. B **54**, 11169 (1996).
[33] J. Heyd, G. E. Scuseria, and M. Ernzerhof, J. Chem. Phys. **118**, 8207 (2003).
[34] J. Heyd, G. E. Scuseria, and M. Ernzerhof, J. Chem. Phys. **124**, 219906 (2006).
[35] A. Gali, Phys. Rev. B **80**, 241204 (2009).
[36] P. Deák, B. Aradi, T. Frauenheim, E. Janzén, and A. Gali, Phys. Rev. B **81**, 153203 (2010).
[37] K. Szász, T. Hornos, M. Marsman, and A. Gali, Phys. Rev. B **88**, 075202 (2013).
[38] J. P. Perdew, K. Burke, and M. Ernzerhof, Phys. Rev. Lett. **77**, 3865 (1996).
[39] V. Ivády, T. Simon, J. R. Maze, I. A. Abrikosov, and A. Gali, Phys. Rev. B **90**, 235205 (2014).
[40] A. L. Falk, P. V. Klimov, B. B. Buckley, V. Ivády, I. A. Abrikosov, G. Calusine, W. F. Koehl, A. Gali, and D. D. Awschalom, Phys. Rev. Lett. **112**, 187601 (2014).
[41] J. Davidsson, V. Ivády, R. Armiento, N. T. Son, A. Gali, and I. A. Abrikosov, arXiv:1708.04508.
[42] See Supplemental Material at http://link.aps.org/supplemental/10.1103/PhysRevB.96.161114 for information about the conditions of EPR measurements and additional data in 6H-SiC.
[43] X. T. Trinh, K. Szász, T. Hornos, K. Kawahara, J. Suda, T. Kimoto, A. Gali, E. Janzén, and N. T. Son, Phys. Rev. B **88**, 235209 (2013).
[44] N. T. Son, P. Carlsson, J. ul Hassan, B. Magnusson, and E. Janzén, Phys. Rev. B **75**, 155204 (2007).
[45] The hyperfine constants of C_{Ia} nuclei are within 0.6% associated with the two sites, which is too small a difference for a decisive conclusion. However, this difference is significant for the other nuclei.
[46] K. Szász, X. T. Trinh, N. T. Son, E. Janzén, and A. Gali, J. Appl. Phys. **115**, 073705 (2014).